

Product Selectivity Controlled by Zeolite Crystals in Biomass Hydrogenation over a Palladium Catalyst

Chengtao Wang,[†] Liang Wang,^{*,†} Jian Zhang,[†] Hong Wang,[‡] James P. Lewis,[‡] and Feng-Shou Xiao^{*,†,§}

[†]Key Lab of Applied Chemistry of Zhejiang Province, Department of Chemistry, Zhejiang University, Hangzhou 310028, China

[‡]Department of Physics, West Virginia University, Morgantown, West Virginia 26506-6315, United States

[§]Key Lab of Biomass Chemical Engineering of Ministry of Education, Zhejiang University, Hangzhou 310027, China

Supporting Information

ABSTRACT: This work delineates the first example for controlling product selectivity in metal-catalyzed hydrogenation of biomass by zeolite crystals. The key to this success is to combine the advantages of both Pd nanoparticles (highly active sites) and zeolite micropores (controllable diffusion of reactants and products), which was achieved from encapsulation of the Pd nanoparticles inside of silicalite-I zeolite crystals as a core-shell structure (Pd@S-1). In the hydrogenation of biomass-derived furfural, the furan selectivity over the Pd@S-1 is as high as 98.7%, outperforming the furan selectivity (5.6%) over conventional Pd nanoparticles impregnated with S-1 zeolite crystals (Pd/S-1). The extraordinary furan selectivity in the hydrogenation over the Pd@S-1 is reasonably attributed to the distinguishable mass transfer of the hydrogenated products in the zeolite micropores.

Selective transformation of renewable biomass-derived feedstocks plays a key role in sustainable production of biofuels and fine chemicals.^{1–10} Up to now, many economically viable processes have been developed for the conversion of biomass.^{6–10} For example, pyrolysis or hydration of lignin and cellulose, which contain more than 30% of the organic carbon on earth, to produce various platform chemicals of phenols, levulinic acids, and furfurals has been deemed to be promising alternatives to crude oil.^{11–15} In these processes, it is notable that the biomass-derived chemicals normally have relatively high oxygen content, which strongly limits their applications.^{11–15} Therefore, upgrading the biomass-derived chemicals by hydrogenation to selectively remove the oxygen groups in the chemicals is strongly desirable. However, it still is a challenge to control the product selectivity in biomass hydrogenation yet because these reaction pathways with many undesirable reactions are very complex.

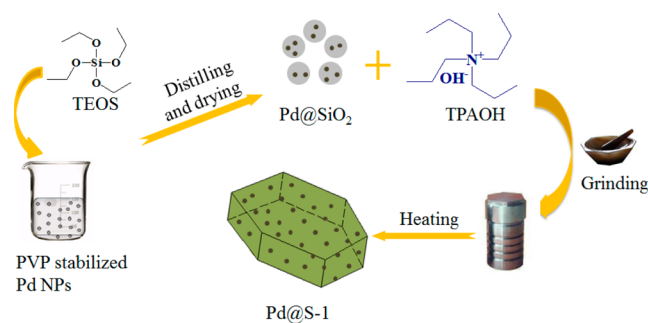
The transition-metal nanoparticles have been widely applied in the hydrogenation of biomass.^{16–19} In these cases, it is not easy to control the product selectivity because the hydrogenation directly occurs on the exposed metal active sites. On the other hand, it is well-known that the mass transfer in catalytic conversion of hydrocarbons is very sensitive to the product selectivity.^{20–23} Typically, introduction of mesoporosity in zeolite crystals and modification of catalyst wettability significantly changes the diffusion of reactants and products,^{21–23} finally enhancing the product selectivity in catalytic

conversion. However, rare efficient strategies exist so far, which allow for rationally controlling the diffusion of reactants and products in metal-catalyzed hydrogenations.

Here we report a generalized strategy for preparation of excellently selective and highly active catalysts by encapsulation of metal nanoparticles inside of microporous silicalite-I (S-1) zeolite as core-shell structures (metal@zeolite), where the metal nanoparticles serve as catalytically active sites and the zeolite micropores control the product selectivity by changing molecular diffusion. Considering that Pd nanoparticles are highly active but poorly selective in the biomass hydrogenation and that S-1 zeolite is easily synthesized, a Pd@S-1 was successfully prepared from solvent-free crystallization of a solid mixture including Pd nanoparticles, amorphous silica, and organic structural directing agent.²⁴ As expected, the Pd@S-1 is highly active and excellently selective in the hydrogenation of biomass derived furfural, giving furan selectivity as high as 98.7% with furfural conversion of 91.3%. In contrast, conventionally supported catalysts show relatively low furan selectivities, which are due to the complexity of reactive pathways and difficulty in controlling the selectivity (Scheme S1).

Scheme 1 shows the procedure for synthesis of the Pd@S-1. At first, the Pd nanoparticle was encapsulated with amorphous SiO₂ obtained from controllable hydrolysis of tetraethyl orthosilicate in polyvinylpyrrolidone-stabilized Pd nanoparticle solution, followed by addition of tetrapropyl ammonium hydroxide solution. After grinding at room temperature in air, the solid mixture was transferred into an autoclave for

Scheme 1. Synthesis of Pd@S-1 Catalyst



Received: May 13, 2016

Published: June 16, 2016

crystallization at 180 °C for 3 days. After washing with water, drying at 100 °C, and calcining at 550 °C for 4 h, the Pd@S-1 was finally obtained. The Pd loading was calculated at 0.34% by ICP analysis. For comparison, the Pd nanoparticles supported on S-1 and Al₂O₃ by impregnation method were denoted as Pd/S-1 and Pd/Al₂O₃ with similar Pd loadings at 0.33% and 0.31%, respectively.

It is worth mentioning that the solvent-free crystallization plays a critical role for the successful preparation of Pd@S-1, which offers a possibility to fully encapsulate the Pd nanoparticles inside of S-1 single crystals. If the Pd nanoparticles are directly exposed to the external surface of the catalysts prepared from other routes such as conventional hydrothermal synthesis of zeolites, the product selectivity in the biomass hydrogenation should be reduced significantly.

Figure S1 shows XRD patterns of various samples. The Pd@S-1 and Pd/S-1 exhibit XRD peaks associated with typical MFI zeolite structure. Notably, it is difficult to observe the peaks associated with metallic Pd crystals, indicating high dispersion and low loading of Pd nanoparticles on/in the samples. Figure S2 shows N₂ sorption isotherms of the S-1, Pd@S-1, and Pd/S-1 samples. They give high surface areas (BET 346–450 m²/g) and large pore volumes (0.14–0.18 m³/g, Table S1), indicating the successful formation of zeolite crystals.

Figure 1 shows tomogram-section transmission electron microscopy (TEM) tomography images of the Pd@S-1 and

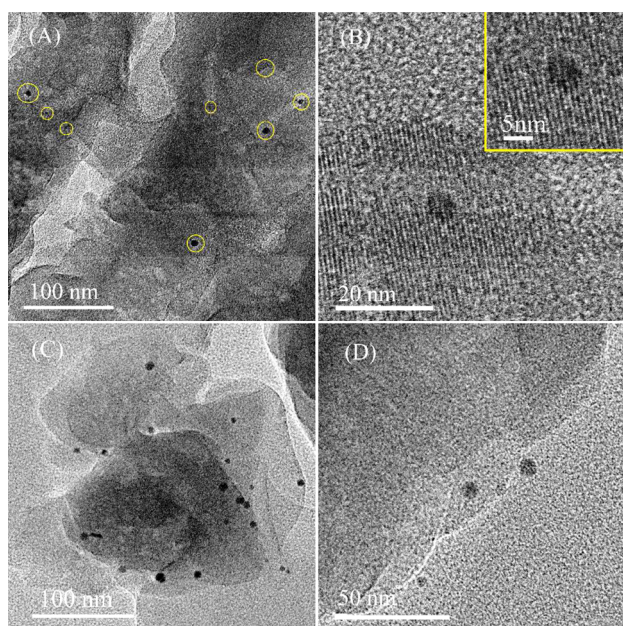


Figure 1. Tomogram-section TEM images of (A and B) the Pd@S-1 and (C and D) Pd/S-1. Insert in B: Enlarged view.

Pd/S-1. This technology offers the sectioned view of the sample, thus avoiding the influence of metal nanoparticles on the external surface. In the Pd@S-1, the Pd nanoparticles could be directly observed (Figure 1A), confirming these nanoparticles are indeed encapsulated within the S-1 zeolite crystals as the core–shell structure. It is shown that the size of Pd nanoparticles in the Pd@S-1 ranged from 3.7 to 11.7 nm with a mean size at 6.9 nm (Figure S3A). In the sectioned view of the Pd/S-1, the Pd nanoparticles are found only on the side of S-1 crystals, indicating that the Pd nanoparticles are located only on the external surface of the S-1 crystals. By counting more than

100 nanoparticles, the nanoparticle size of the Pd/S-1 is calculated at 4.1–10.9 nm (Figure S3B), which is similar to those of the Pd@S-1 and Pd/Al₂O₃ (Figures S3A and S4).

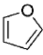
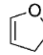
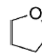
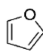
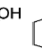
Furthermore, the structure of the Pd@S-1 was investigated by hydrogenation of probing molecules such as benzaldehyde (BA) and 3,5-isopropylbenzaldehyde (DPBA) with different molecular diameters. Table S2 presents the catalytic data in the hydrogenation of mixed substrates of BA and DPBA over the Pd@S-1, Pd/S-1, and Pd/Al₂O₃. Notably, these catalysts are active for the hydrogenation of BA (61–100%). However, for the hydrogenation of DPBA, the Pd/S-1 and Pd/Al₂O₃ are still active, but the Pd@S-1 is completely inactive. This phenomenon is assigned to the molecule diameter of DPBA which is obviously larger than the size of the S-1 micropores, making the DPBA molecules difficult to access to the Pd nanoparticles through the microporous channels. On the contrary, the Pd/S-1 and Pd/Al₂O₃ are very active in the hydrogenation of DPBA because the Pd nanoparticles are directly exposed on the external surface of the catalysts. These results confirm that the Pd nanoparticles are fully encapsulated inside of the S-1 crystals, forming the Pd@S-1 as a core–shell structure.

Table 1 presents catalytic data in hydrogenation of furfural over the Pd@S-1 and Pd/S-1 in a fixed-bed reactor. The major products include furan, dihydrofuran, tetrahydrofuran, and furfuryl alcohols. Because furan is a promising platform chemical, it is always desirable to get high selectivity in the furfural hydrogenation. However, the conventional Pd catalysts normally show relatively low selectivity for the furan, which is due to the difficulty in the selective cleavage the C–C bond of the furfural.^{19,25,26} Notably, the Pd@S-1 and Pd/S-1 are very active for the furfural hydrogenation, but their furan selectivities are quite different (Figure S5). For example, when the reaction was carried out at 250 °C, the Pd@S-1 exhibits the selectivity for furan as high as 98.7% with furfural conversion at 91.3% (entry 5), which is much higher than those of industrial Pd/Al₂O₃ catalyst (Table S3) and the catalysts reported previously.¹⁹ In this case, it has also detected CO, CO₂, and HCOH formed by C–C cleavage of furfural, Figure S6). In contrast, the Pd/S-1 gives similar conversion (91.4%), but very low furan selectivity (5.6%, entry 11). In addition, a large amount of bulky molecules from the condensation of the furfural are detectable (selectivities at 33.7–75.7%, entries 7–12). Possibly, these bulky molecules could be formed on the exposed Pd surface over the Pd/S-1, while these molecules are difficult to form in the zeolite micropores with sizes of ~0.55 nm over the Pd@S-1.

Considering that the Pd@S-1 and Pd/S-1 have similar Pd loading, nanoparticle size distribution, and the same S-1 zeolite support, it is reasonably suggested that the high furan selectivity over the Pd@S-1 should be directly attributed to the core–shell structure rather than other factors. To confirm this suggestion, HF treatment of the Pd@S-1 was carried out. After partial destruction of the S-1 zeolite framework in the Pd@S-1 (Figure S7), the treated Pd@S-1-HF gives a significant reduction of furan selectivity (46.2%, entry 13), compared with the Pd@S-1 (98.7%, entry 5). This result demonstrates the importance of the S-1 zeolite as a shell for controlling the furan selectivity in the furfural hydrogenation over the Pd@S-1.

The difference in diffusion of reactants and products in the hydrogenation was monitored by FT-IR spectra of the adsorbed molecules on the Pd@S-1 at first. After desorption under the same conditions, the intensity of the band at ~1227 cm⁻¹, associated with the C–O bond in the furan or

Table 1. Catalytic Data in Furfural Hydrogenation over Various Catalysts^a

Entry	Catalyst	Temp. (°C)	Conv. (%)	Selectivity (%)						Balance ^c
									Others ^b	
1	Pd@S-1	150	29.1	86.5	3.9	9.6	0	0	0	1.07
2	Pd@S-1	175	50.7	91.8	3.1	5.1	0	0	0	0.98
3	Pd@S-1	200	83.7	95.7	1.4	2.9	0	0	0	0.99
4	Pd@S-1	225	88.9	96.8	1.9	1.3	0	0	0	1.03
5	Pd@S-1	250	91.3	98.7	0.8	0.5	0	0	0	1.03
6	Pd@S-1	275	80.0	77.9	0.3	0.3	0	0	21.5	1.06
7	Pd/S-1	150	43.0	7.0	28.0	20.5	7.0	0	37.5	1.08
8	Pd/S-1	175	44.2	13.5	11.5	31.7	9.6	0	33.7	0.87
9	Pd/S-1	200	63.5	11.3	2.2	18.9	7.6	0	60.0	0.91
10	Pd/S-1	225	89.0	8.1	1.6	11.6	13.2	0	65.5	0.88
11	Pd/S-1	250	91.4	5.6	1.1	12.3	12.7	0	68.3	0.93
12	Pd/S-1	275	96.7	6.9	0	13.2	4.2	0	75.7	1.02
13	Pd@S-1-HF ^d	250	81.0	46.2	0	11.1	40.1	2.6	0	0.98

^aReaction condition: 5 wt % furfural (mass ratio of furfural/*n*-butyl alcohol at 1:19), feed rate at 0.5 mL/h, 10% H₂/Ar at a rate of 10 mL/min, 100 mg of catalyst, 1 atm pressure. ^bBulky molecules from the condensation of furfural. ^cMolecular balance during the reaction, calculated from the amount of furan and tetrahydrofuran rings in feeds and products. ^dHF-treated Pd@S-1 was used as catalyst.

tetrahydrofuran rings of these molecules, could be reduced in the Pd@S-1 (Figure S8). By analyzing a change in the band intensity (Table S4), the desorption percentages for the 1227 cm⁻¹ band intensities of various molecules are calculated, as summarized in Figure 2A. Clearly, desorption of more

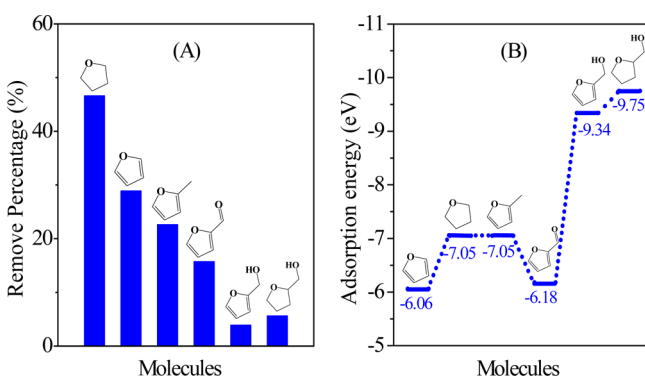


Figure 2. (A) The percentage of various molecules removed from Pd@S-1 during the same desorption treatment. (B) Calculated adsorption energy for each molecule in the micropores of the S-1 zeolite.

molecules means faster molecular diffusion in the S-1 micropores. Interestingly, the desorption percentage of furan (46.6%) is much more than that of furfural, furfuryl alcohol, tetrahydrofuran, tetrahydrofurfuryl alcohol, and methylfuran (3.9–28.9%). These results suggest that the furan has a much faster diffusion rate than that of the other molecules in the micropores of the Pd@S-1. Further evidence for faster diffusion rate of the furan than that of the other molecules in the S-1 micropores is given by the temperature-programmed desorption (TPD) measurements of these molecules (Figure S9).

Understanding of diffusion behavior of various molecules in the micropores of S-1 zeolite was also achieved by theoretical simulation. Figure S10 shows the models of furfural, furan, furfuryl alcohol, tetrahydrofuran, tetrahydrofurfuryl alcohol, and methylfuran localized in the microporous channels of the S-1 zeolite, and their calculated adsorption energies (E_{ads}) for various molecules are shown in Figure 2B. The E_{ads} for per furan molecule is -6.06 eV, which has lower absolute value

than those of furfural (-6.18 eV), furfuryl alcohol (-9.34 eV), tetrahydrofuran (-7.05 eV), tetrahydrofurfuryl alcohol (-9.75 eV), and methylfuran (-7.05 eV). These results indicate that the zeolite microporous channels tend to adsorb the furan molecule much more weakly than the other molecules, suggesting that the furan molecules tend to diffuse faster through the zeolite micropores than that of the other molecules, in good agreement with those obtained from IR spectroscopy (Figure S8 and Table S4) and TPD measurements (Figure S9).

Based on these results, it is proposed that, for example, if furfuryl alcohol was formed from the furfural hydrogenation, which is a major side reaction paralleling with the decarbonylation to directly form furan,^{19,25} it tends to be localized on the Pd sites by strong adsorption in zeolite micropores, thus leading to further reaction until to form easily diffused furan molecule (Table S5). This proposed mechanism could also be confirmed by the fact that the furfuryl alcohol was completely undetectable over the Pd@S-1, due to the strong adsorption ability of micropores to this molecule. In contrast, the furfuryl alcohol is always formed over the Pd/S-1 and Pd/Al₂O₃ catalyst (Tables 1 and S3), because of the lack of zeolite micropores on the Pd surface.

Figure 3 shows the dependence of furfural conversion and furan selectivity on reaction time over the Pd@S-1. The catalyst retains its activity and selectivity in the period of 8 h, then reduces the furfural conversion. After calcination at 550 °C for

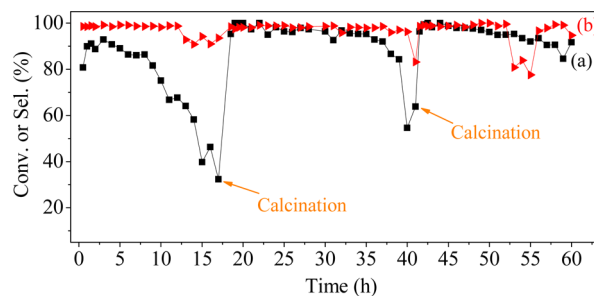


Figure 3. Dependence of (a) conversion of furfural and (b) selectivity of furan over the Pd@S-1 in hydrogenation of furfural to furan.

3 h in oxygen flowing, the Pd@S-1 completely regenerated its catalytic property by removing the coke in the catalyst (Figure S11). Even if the reaction time reaches to 60 h, the Pd@S-1 still keeps similar furfural conversion and furan selectivity to the fresh catalyst. TEM image of the Pd@S-1 reacted for 60 h shows that the size distribution of Pd nanoparticles is very similar to those of the fresh catalyst (Figure S12), indicating that high regenerated activity and selectivity should be from good stability of these Pd nanoparticles during the hydrogenated process. Even with calcination of the Pd@S-1 at 600 °C for 4 h in air, the Pd nanoparticles still keep their Pd size distribution (Figure S13). In comparison, most of the Pd nanoparticles on the external surface of S-1 zeolite aggregate to larger than 10 nm nanoparticles after the same treatment (Figure S14). This phenomenon could be assigned to the unique core-shell structure of Pd@S-1 zeolite, where the S-1 shell prevents the aggregation of Pd nanoparticles.^{27–29}

It is worth noting that the strategy of controlling product selectivity by zeolite crystals is not only applied to Pd nanoparticles but also to Ru and Pt nanoparticles. For example, in the selective hydrogenation of furfural to furan, the S-1 zeolite encapsulated Ru and Pt nanoparticles are also synthesized by the solvent-free route (Figures S15 and S16), significantly exhibiting higher furan selectivity than the Ru and Pt nanoparticles on the external surface of S-1 crystals (Tables S6 and S7).

In summary, we show a novel strategy to control the furan selectivity in the furfural hydrogenation over a core-shell structural Pd@S-1 catalyst synthesized from a solvent-free crystallization. This catalyst efficiently combines high activity of the Pd nanoparticles and excellent selectivity of zeolite micropores, giving the furan selectivity as high as 98.7% with furfural conversion at 91.3%. In addition, this catalyst is easily regenerated by calcination at 550 °C. The strategy for preparation of the Pd@S-1 with high activity, excellent selectivity, and superior regenerated activity in the furfural hydrogenation is potentially important for designing and developing highly efficient heterogeneous catalysts in the future.

■ ASSOCIATED CONTENT

Supporting Information

The Supporting Information is available free of charge on the ACS Publications website at DOI: 10.1021/jacs.6b04951.

Experimental details and data (PDF)

■ AUTHOR INFORMATION

Corresponding Authors

*liangwang@zju.edu.cn

*fsxiao@zju.edu.cn

Notes

The authors declare no competing financial interest.

■ ACKNOWLEDGMENTS

This work is supported by National Natural Science Foundation of China (21333009, U1462202, and 21403192).

■ REFERENCES

(1) Zhang, X.; Liu, D.; Xu, D.; Asahina, S.; Cychosz, K. A.; Agrawal, K. V.; Al Wahedi, Y.; Bhan, A.; Al Hashimi, S.; Terasaki, O.; Thommes, M.; Tsapatsis, M. *Science* **2012**, *336*, 1684–1687.

(2) Lew, C. M.; Rajabbeigi, N.; Tsapatsis, M. *Microporous Mesoporous Mater.* **2012**, *153*, 55–58.

(3) Chang, C.; Green, S. K.; Williams, C. L.; Dauenhauer, P. J.; Fan, W. *Green Chem.* **2014**, *16*, 585–588.

(4) Xia, Q.-N.; Cuan, Q.; Liu, X.-H.; Gong, X.-Q.; Lu, G.-Z.; Wang, Y.-Q. *Angew. Chem., Int. Ed.* **2014**, *53*, 9755–9760.

(5) Su, D. S.; Perathoner, S.; Centi, G. *Chem. Rev.* **2013**, *113*, 5782–5816.

(6) Román-Leshkov, Y.; Barrett, C. J.; Liu, Z. Y.; Dumesic, J. A. *Nature* **2007**, *447*, 982–986.

(7) Do, P. T. M.; McAtee, J. R.; Watson, D. A.; Lobo, R. F. *ACS Catal.* **2013**, *3*, 41–46.

(8) Lam, E.; Luong, J. H. T. *ACS Catal.* **2014**, *4*, 3393–3410.

(9) Román-Leshkov, Y.; Moliner, M.; Labinger, J. A.; Davis, M. E. *Angew. Chem., Int. Ed.* **2010**, *49*, 8954–8957.

(10) Yang, J.; Li, N.; Li, S.; Wang, W.; Li, L.; Wang, A.; Wang, X.; Cong, Y.; Zhang, T. *Green Chem.* **2014**, *16*, 4879–4884.

(11) Corma, A.; Iborra, S.; Velty, A. *Chem. Rev.* **2007**, *107*, 2411–2502.

(12) Liu, D. J.; Chen, E. Y.-X. *ACS Catal.* **2014**, *4*, 1302–1310.

(13) Chheda, J. N.; Huber, G. W.; Dumesic, J. A. *Angew. Chem., Int. Ed.* **2007**, *46*, 7164–7183.

(14) Wang, H. M.; Male, J.; Wang, Y. *ACS Catal.* **2013**, *3*, 1047–1070.

(15) Peng, B.; Yao, Y.; Zhao, C.; Lercher, J. A. *Angew. Chem., Int. Ed.* **2012**, *51*, 2072–2075.

(16) Corma, A.; Iborra, S.; Velty, A. *Chem. Rev.* **2007**, *107*, 2411–2502.

(17) Schrader, I.; Warneke, J.; Backenkohler, J.; Kunz, S. *J. Am. Chem. Soc.* **2015**, *137*, 905–912.

(18) Pang, S. H.; Schoenbaum, C. A.; Schwartz, D. K.; Medlin, J. W. *Nat. Commun.* **2013**, *4*, 2448.

(19) Zhang, H.; Gu, X.-K.; Canlas, C.; Kropf, A. J.; Aich, P.; Greeley, J. P.; Elam, J. W.; Meyers, R. J.; Dumesic, J. A.; Stair, P. C.; Marshall, C. L. *Angew. Chem., Int. Ed.* **2014**, *53*, 12132–12136.

(20) Ma, X.; Zhou, A.; Song, C. *Catal. Today* **2007**, *123*, 276–284.

(21) Liu, F.; Willhammar, T.; Wang, L.; Zhu, L.; Sun, Q.; Meng, X.; Carrillo-Cabrera, W.; Zou, X.; Xiao, F.-S. *J. Am. Chem. Soc.* **2012**, *134*, 4557–4560.

(22) Dai, C.; Zhang, A.; Liu, M.; Guo, X.; Song, C. *Adv. Funct. Mater.* **2015**, *25*, 7479–7487.

(23) Liu, F.; Wang, L.; Sun, Q.; Zhu, L.; Meng, X.; Xiao, F.-S. *J. Am. Chem. Soc.* **2012**, *134*, 16948–16950.

(24) Ren, L.; Wu, Q.; Yang, C.; Zhu, L.; Li, C.; Zhang, P.; Zhang, H.; Meng, X.; Xiao, F.-S. *J. Am. Chem. Soc.* **2012**, *134*, 15173–15176.

(25) Bhogeswararao, S.; Srinivas, D. *J. Catal.* **2015**, *327*, 65–77.

(26) Pang, S. H.; Schoenbaum, C. A.; Schwartz, D. K.; Medlin, J. W. *ACS Catal.* **2014**, *4*, 3123.

(27) Laursen, A. B.; Højholt, K. T.; Lundegaard, L. F.; Simonsen, S. B.; Helveg, S.; Schuth, F.; Paul, M.; Grunwaldt, J.-D.; Kegncs, S.; Christensen, C. H.; Egeblad, K. *Angew. Chem., Int. Ed.* **2010**, *49*, 3504.

(28) Goel, S.; Zones, S. I.; Iglesia, E. *J. Am. Chem. Soc.* **2014**, *136*, 15280–15290.

(29) Mielby, J.; Abildstrøm, J. O.; Wang, F.; Kasama, T.; Weidenthaler, C.; Kegncs, S. *Angew. Chem., Int. Ed.* **2014**, *53*, 12513.